PEER-REVIEWED ARTICLE

Leveraging robotic total stations and multi-sensor adjustment for accurate multibeam bathymetry

Authors

Lucas Dammert[1], Florian Pöppl[2], Jan Rhomberg-Kauert[1], Tomas Thalmann[1], David Monetti[3], Hans-Berndt Neuner[1] and Gottfried Mandlburger[1]

Abstract

In our study we geo-reference a multibeam echosounder (MBES) data set with a robotic total station (RTS). We use this data to perform a multi-sensor least-squares adjustment that leverages planar correspondences within the MBES data to estimate the trajectory. We compare this to GNSS-based processing and conventional direct geo-referencing. Our results show that the adjustment improves the precision from an interquartile range of 8 cm to 4 cm. Also, the height residuals of the trajectory adjustment can be reduced to 1 mm with RTS-based positioning versus 12 mm with GNSS. When the RTS-based MBES dataset is compared with bathymetric LiDAR, the standard deviation is 4 cm, and the median difference is -1 cm. Our approach offers improved accuracy and precision compared to GNSS-based systems and can also be used in GNSS-challenged environments such as mountainous regions or next to quay walls.

Keywords

bathymetric LiDAR · hydrography · MBES · RTS · trajectory

Resumé

Dans notre étude, nous géoréférençons un ensemble de données provenant d'un sondeur multifaisceaux (MBES) à l'aide d'une station totale robotisée (RTS). Nous utilisons ces données pour effectuer un ajustement multicapteur par la méthode des moindres carrés qui exploite les correspondances planes dans les données MBES afin d'estimer la trajectoire. Nous comparons cette méthode à un traitement se basant sur le GNSS et au géoréférencement direct conventionnel. Nos résultats montrent que l'ajustement améliore la précision, passant d'un intervalle interquartile de 8 cm à 4 cm. De plus, les résidus de hauteur de l'ajustement de la trajectoire peuvent être réduits à 1 mm avec le positionnement basé sur le RTS, contre 12 mm avec le GNSS. Lorsque le jeu de données MBES basé sur le RTS est comparé au LiDAR bathymétrique, l'écart type est de 4 cm et la différence médiane est de -1 cm. Notre approche offre une précision et une exactitude améliorées par rapport aux systèmes qui se basent sur le GNSS et peut également être utilisée dans des environnements difficiles pour le GNSS, tels que les régions montagneuses ou à proximité des murs de quai.

Resumen

En nuestro estudio georreferenciamos un conjunto de datos de una ecosonda multihaz (MBES) con una estación total robótica (RTS). Usamos estos datos para realizar un ajuste multisensor por mínimos cuadrados que aprovecha las correspondencias planares dentro de los datos MBES para estimar la trayectoria. Lo comparamos con el procesamiento basado en GNSS y la georreferenciación directa convencional. Nuestros resultados muestran que el ajuste mejora la precisión desde un rango intercuartil de 8 cm a uno de 4 cm. Además, se pueden reducir los residuos de altura del ajuste de trayectoria a 1 mm con el posicionamiento basado en RTS, frente a los 12 mm con GNSS. Cuando se compara el conjunto de datos MBES basado en RTS con el LiDAR batimétrico, la desviación estándar es de 4 cm, y la mediana de la diferencia es de -1 cm. Nuestro enfoque ofrece una mayor exactitud y precisión en comparación con los sistemas basados en GNSS, y también se puede utilizar en entornos difíciles para GNSS, como regiones montañosas o junto a muros de contención.

✉ Lucas Dammert · lucas.dammert@geo.tuwien.ac.at

[1] TU Wien, Department of Geodesy and Geoinformation, 1040 Vienna, Austria

[2] *RIEGL* Laser Measurement Systems GmbH, 3580 Horn, Austria

[3] Skyability GmbH, GZO-Dienstleistungszentrum 5, 7011 Siegendorf, Austria

https://doi.org/10.58440/ihr-31-2-a14

1 Introduction

Bathymetric mapping of water bodies is a topic that becomes increasingly relevant, e.g. in the context of climate change and environmental research (Mandlburger et al., 2025; Mokhtar et al., 2023). The development of uncrewed surface vehicles (USVs) facilitates the surveying of inland water bodies with Sound Navigation and Ranging (SONAR). Meanwhile, the ranging accuracy of SONAR reaches the cm-level for shallow water depths (Ernstsen et al., 2006; Norbit Subsea, 2021), comparable to bathymetric LiDAR (Light Detection and Ranging) sensors (Mandlburger et al., 2025; RIEGL, 2021). Similar to topographic LiDAR (Dammert et al., 2025b), the geo-referencing of the SONAR data with Real-Time Kinematic (RTK) GNSS accounts for a large part of the error budget of the resulting point cloud. Thus, the GNSS-RTK trajectory can limit the overall accuracy of multi-sensor systems consisting of SONAR, GNSS, and Inertial Measurement Unit (IMU) (Skaloud & Lichti, 2006; Dammert et al., 2025a, 2025b). Consequently, a more accurate trajectory can directly improve the overall accuracy of the multi-sensor system. Especially GNSS-derived heights exhibit low accuracy (Möser et al., 2012; Krzyzek and Kudrys, 2022), while quality standards, such as the International Hydrographic Office's IHO S-44, emphasize vertical accuracy requirements over horizontal accuracy requirements (IHO, 2022). For example, the IHO S-44 Special Order and Exclusive Order require Total Horizontal Uncertainty (THU) values of 2 m and 1 m respectively, while the required Total Vertical Uncertainty (TVU) value is, e.g. at a water depth of 20 m, 0.29 m and 0.17 m respectively. While the magnitude of these values varies depending on the Order and water depth, the general relationship between THU and TVU is apparent: The vertical uncertainty requirement is more strict than the horizontal uncertainty requirement.

This motivates two research questions, which we address in our publication: (i) Can Robotic Total Stations (RTS) improve the geo-referencing accuracy, in particular the height, of bathymetric point clouds compared to GNSS, and what impact does the trajectory estimation strategy have on the precision of our data set? (ii) how consistent is our RTS-based data with Airborne Laser Bathymetry (ALB) data?

Modern RTS allow reliable position measurements of kinematic platforms, with measurement rates of up to 20 Hz and uncertainties below 1 cm (Dammert et al., 2025a). Thus, RTS outperform GNSS-based positioning systems in accuracy (Dammert et al., 2025b) and often also in sampling rate. Measurements of RTS are initially obtained in a local coordinate frame. This usually requires an additional transformation of the measured positions in a global coordinate frame based on reference points which are known in this global coordinate frame. However, the accuracy of transformed RTS measurements is generally higher than that of kinematic GNSS-RTK measurements, as the transformation parameters can be estimated based on more accurate, static GNSS observations (millimetre level with sufficient observation time) compared to kinematic GNSS measurements (low centimetre level) onboard the survey vehicle (Möser et al., 2012). In addition, the RTS allows a higher accuracy of the data set's inner geometry as any transformation uncertainties affect the complete data set in the same way. In general, the application of RTS offers the possibility of reducing the influence of inaccurate trajectory information and results in an improved (bathymetric) point cloud. Although most publications focus on terrestrial platforms (Vaidis et al., 2023; Kälin et al., 2023; Kerekes & Schwieger, 2018) or airborne platforms (Dammert et al., 2025b; Maxim et al., 2017), RTS-based positioning of water surface vehicles has also been subject to discussion (Hesse et al., 2021; Popielarczyk, 2016) but lacks a detailed investigation of its achievable uncertainties and advantages. However, RTS can only measure the position of the multi-sensor system and require IMU data for additionally obtaining the platform's orientation (roll, pitch, and yaw) and, thus, a full 6-Degree-of-Freedom (DoF) trajectory estimation, which consists of three translation and three rotation elements.

In this study, we present a hardware-based approach using RTS measurements to geo-reference a multibeam echosounder (MBES) multi-sensor system. The general idea, already described in Hesse et al. (2021) and in Popielarczyk (2016), is motivated by the high measurement accuracy of RTS and their independence from GNSS multipath effects and signal obstructions, e.g., by quay walls, trees, and mountains or, more recently, signal jamming. Recent studies show that, in particular, the height accuracy of RTS offers superior accuracy compared to GNSS (Dammert et al., 2025b; Popielarczyk, 2016).

The integration of time-synchronized RTS data with the onboard data of the survey vessel, namely IMU and MBES, to obtain 6-DoF trajectories is also a topic of recent research. Classic sensor integration for hydrographic multi-sensor systems employs real-time Kalman Filtering based on position information measured by GNSS and the attitude data of an IMU to estimate the trajectory of the system (Groves, 2013). In post-processing, these trajectories are usually refined by employing Post-Processed Kinematic (PPK) GNSS and replacing the sequential filter by a forward-backward smoother (Gong et al., 2013). The data of the mapping sensor, e.g. MBES, is directly geo-referenced with this trajectory, leading to a geo-referenced 3D point cloud. Recent work on Kalman Filtering for RTS data makes direct use of the polar elements observed by the RTS enabling tight coupling with IMU data and allowing separate evaluation of distance and angle measurements (Thalmann & Neuner, 2024). Although they present the example of a tilt compensating prism pole in their work, the concept can easily be transferred to multi-sensor systems in general.

https://doi.org/10.58440/ihr-31-2-a14

To fully leverage the potential of highly accurate trajectory information by RTS, we use a state-of-the-art software-based approach originating from airborne laser scanning (ALS) which leverages correspondences in the point cloud to optimize the trajectory estimation. For this, we make use of the multi-sensor trajectory estimation approach described by Pöppl et al. (2024) integrating GNSS, IMU, and LiDAR measurements, and adapt it by replacing GNSS with RTS positions and LiDAR data with MBES data.

This multi-sensor adjustment enables, in addition to the estimation of the 6-DoF trajectory and the IMU errors, the reliable estimation of boresight and lever arm parameters based on the complete data set. Therefore, the traditional misalignment calibration using a Patch Test (Gueriot et al., 2000), which usually focusses on (manually) aligning only a small part of the survey data to estimate the angular offsets of the MBES sensor head, is here replaced by a numerical approach that considers the complete available data set. This shift toward numerical, algorithmic methods which make use of the complete data set is further supported by the advantages outlined in Le Deunf et al. (2020) and Skaloud & Lichti (2006). Among the most important advantages are the increased objectivity and repeatability of this automated calibration. In addition, the least-squares-based approach has, due to the use of the complete data set, redundancy and can thus provide a measure of precision.

The resulting highly accurate RTS-based MBES data set allows a reliable comparison of the MBES data to ALB data. When using GNSS-based geo-referencing for both, MBES and ALB, the precise registration of both data sets is only possible when using submerged geometric features. For bathymetric data sets the ground is one such feature and structures with diverse orientations as are e.g. available in airborne laser scans of urban scenarios are lacking. The ground is usually nearly horizontal and thus offers little information for the horizontal registration of the point clouds. With our RTS-based MBES data set, we can register the ALB data without relying on submerged geometric features. To minimize the impact of geo-referencing uncertainties on the ALB data, they are indirectly geo-referenced using reference planes in the study area, from which the plane parameters are known based on RTS measurements.

In our contribution, we present a decentralized multi-sensor system consisting of an RTS and an MBES equipped with an IMU together with an integrated geo-referencing approach and thorough evaluation thereof. The three main contributions are: (i) the integration of MBES and RTS with tight IMU coupling, (ii) the assessment of the resulting geo-referenced point cloud compared to an analogously processed GNSS-based data set, and (iii) the comparison of the former data set to an ALB data set.

Our article is structured as follows: Section 2 focuses on the available data sets and the sensors used for data acquisition. In Section 3, we first describe our approach to sensor fusion of RTS and IMU, and GNSS and IMU, respectively (Section 3.1) and then describe the additional integration of MBES data (Section 3.2). We also elaborate on the error exhibited by not adapting the sound velocity correction when optimizing the trajectory. In Section 4, we evaluate the precision of the resulting point clouds and analyse the impact of different swath widths on the precision. We also compare our RTS-based data set with the GNSS-based data set and compare our RTS-based MBES data set with ALB data. We end with a discussion of our results in Section 5.

2 Data set and study area

Our study is based on a data set acquired at Lake Erlauf (Fig. 1) in Austria. The data set consists of data acquired by MBES and ALB. The MBES data used in our study employ a Norbit Winghead i77h MBES (Norbit Subsea, 2021) and are geo-referenced once with RTS and once with GNSS measurements. The setup used is shown in Fig. 2. In addition to the MBES survey, an ALB survey was conducted, where a topo-bathymetric *RIEGL* VQ-840-G sensor was operated from a helicopter platform.

2.1 Robotic total station

In our study, a Leica GRZ-122 360° prism mounted on the boat is used as a target for a Leica MS60 RTS (Zogg & Maar, 2020), which continuously measures the position of the prism. The Leica MS60 RTS is one of the newest RTS from the manufacturer Leica. It features very reliable target tracking, that can track the prism even during fast movement, e.g., in Dammert et al. 2025 this instrument is used to track an airborne platform at speeds of 10 m/s. Our test showed that the tracking of fast targets is reliably possible until about 800 m, depending on the atmospheric conditions. The target tracking requires an unobscured line-of-sight between RTS and target.

In our study, the boat was moving quite slowly and the only observable reason for failure of the target tracking is the appearance of specular reflection of sunlight at the water surface in the image sensor that guides the target tracking. In those situations, the image sensor cannot distinguish the reflection of its emitted laser signal from the prism from the ambient sunlight. If those interruptions remain reasonably short, they can later be bridged by using the IMU data, similar to handling short GNSS outages. However, if the platform, i.e. USV, moves beyond a threshold (depending on the settings of the RTS) during these interruptions, and without real-time communication between the RTS and the platform, the RTS needs to be manually guided to re-establish the target tracking.

To allow for time-synchronized measurements of the RTS, we employ the approach described in Thalmann & Neuner (2021) and Dammert et al. (2025b). It incorporates a controller unit that requests and receives the measurements of the RTS using

https://doi.org/10.58440/ihr-31-2-a14

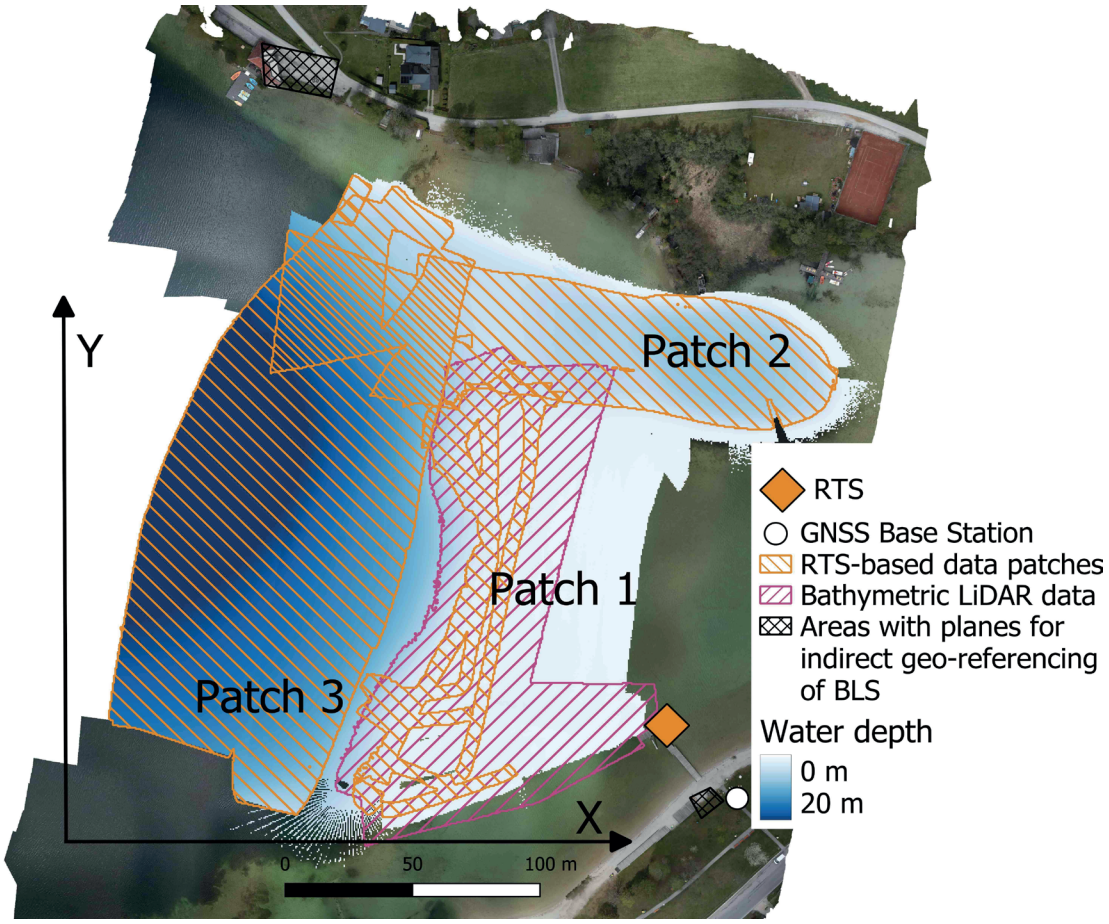


Fig. 1 Map for better spatial orientation within the entire study area, with colour coded water depths from GNSS-based MBES data, extent of MBES data, and ALB data.

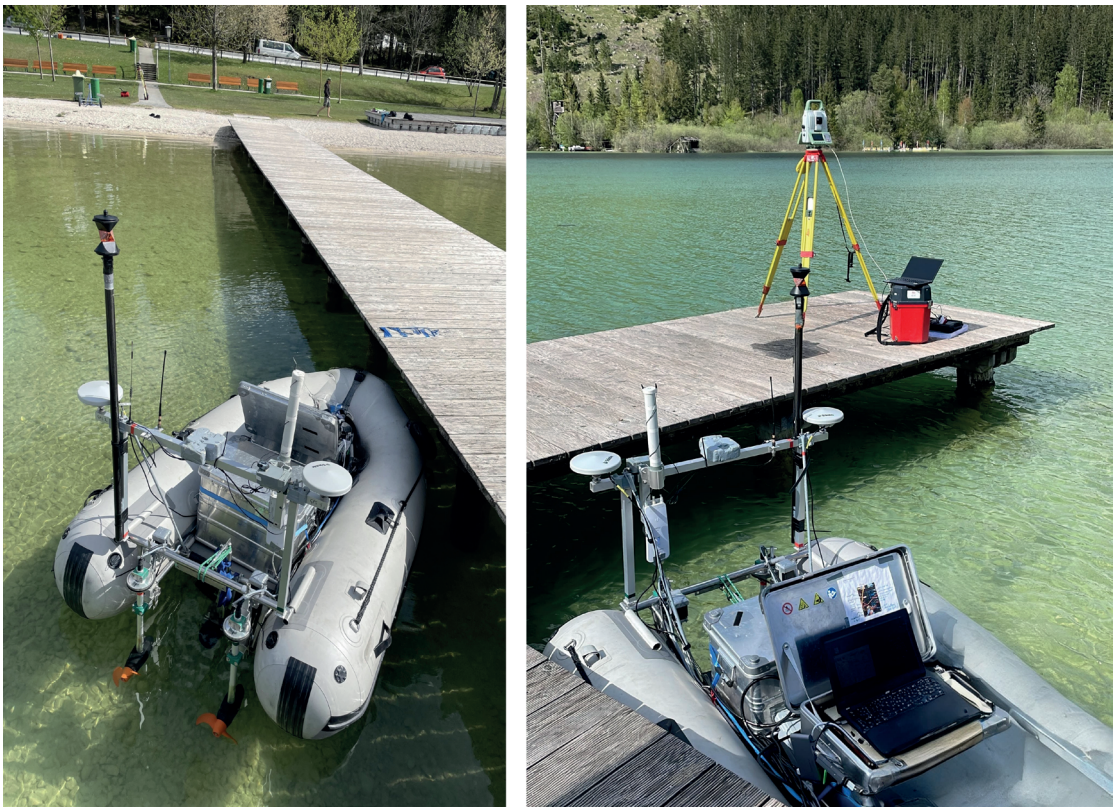


Fig. 2 Setup of the multi-sensor system with RTS, prism, GNSS antennas, and MBES (submerged).

the communication interface of the RTS. For Leica RTS, this interface is called GeoCom. The controller is synchronized with GPS time using a uBlox GNSS receiver that transmits the received NMEA string and the PPS (pulse-per-second) signal to the controller. The temporal offset and drift of the RTS with regard to the synchronized controller are measured in the field, and the exhibited latencies of the setup are calibrated in our laboratory (Thalmann & Neuner, 2021). In general, the RTS has no absolute time information but a relative time system which starts when the instrument is powered on. Thus, the temporal offset yields no meaningful value. However, the drift of this time system, which we identified and corrected for, is about 40 ppm. After application of these parameters, we consider an additional (extrinsic) latency of about 61 ms for the measurements of the Leica MS60.

Our RTS data set is divided into three approximately 10 min to 15 min long patches (Fig. 1). We used the three patches, Patches 1–3, for the evaluation of our data, but due to the limited water depth penetration of the ALB, only one of these patches, Patch 1, is used in Section 4.3 for the comparison between MBES and ALB.

2.2 GNSS

We process the kinematic GNSS data of our hydrographic multi-sensor system in addition to the RTS data and evaluate them in Section 4.2. All GNSS data were acquired in ITRF2020 (Epoch 2015.0), and all heights refer to ellipsoidal heights of the GRS80 ellipsoid. In contrast to the RTS data, the GNSS data was recorded consecutively without interruption, leading to slightly larger coverage. In addition, to transform all data sets into a common coordinate frame, we performed four static GNSS observations of at least 1.5 hours as part of a geodetic network at the study site. During the entire data acquisition, we used the same local base station for all GNSS-related measurements (i.e. MBES and ALB).

2.3 Multibeam echosounder

MBES allow the efficient acquisition of bathymetric data by sending out multiple acoustic beams at different angles. In our study, a NORBIT Winghead i77h is used, allowing the acquisition of 1024 simultaneous beams or measurements in a swath perpendicular to the forward direction of the vessel. The Winghead i77h uses an Applanix Oceanmaster IMU mounted directly on the sensor head of the MBES to record inertial data. In our survey, the beam divergence of the MBES was 0.5° × 0.9° with a point spacing of 2–10 cm across, depending on the water depth, and 12 cm along the trajectory. The range resolution of the sensor is given by the manufacturer with < 10 mm (Norbit Subsea, 2021). We acquired data with a swath width of 180° and limited the swath width to 90° during data processing. In Section 4.1.2 we investigate the effect of different swath widths on the height precision of our data. We use MBES data acquired with QPS Qinsy and pre-processed with QPS Qimera. We rely on the QPS software suite for the sound velocity correction (Section 2.4) and export the initially geo-referenced MBES data together with the used trajectory from the software. From this we transform the data back into the sensor coordinate frame using the OPALS software (Pfeifer et al., 2014) and the transformation parameters used for the initial data acquisition with QPS Qinsy. This data is then used for our processing, e.g. geo-referencing using RTS position information (Section 3).

2.4 Sound velocity data

For processing of the MBES data, we recorded a sound velocity profile (SVP) with a sound velocity profiler in the centre of our study area. The water depth covered by this profile was 14 m and this profile was used for the sound speed correction of the complete data set in the QPS software (Section 2.3). However, we encountered large geometric discrepancies in our data set and found that the surface-near sound velocity, logged by the MBES, varied between 1,444 ms^{-1} to 1,451 ms^{-1} for the surveyed part of Lake Erlauf (Fig. 3). These measurements are taken by a sound velocity profiler, mounted in the MBES sensor head, during the survey which took about two hours. While the surface sound velocity logged by the MBES for the location of our SVP matches the value recorded in our SVP, the surface sound velocities are very heterogeneous. Thus, the measured SVP does not give a good representation of the study area, and the depth measurements at outer beam angles, e.g. greater than 45°, are severely affected by this incorrect modelling of the sound velocity profile. The acquired sound velocity data are visualized in Fig. 3 for better understanding. We see a correlation of the sound velocity with the extent of the underlying water column as the survey took place in the evening, where the shallow parts of the lake were already heated by the sun. In addition, the Lake drains into a small river on the northeastern part, causing potential differences in the water column due to the flow of fresh water. We find that this variation in the surface sound velocity can, when assuming a constant temperature gradient, impact our depth measurements by up to 2 cm. In Section 4.1 we also elaborate on the effect of different swath widths on the quality of the data set.

2.5 Bathymetric LiDAR

For the acquisition of bathymetric LiDAR data, a *RIEGL* VQ840-G was used in our field campaign. The sensor was mounted on a helicopter with a flying altitude of 100 m. For the initial processing of the bathymetric LiDAR data, the manufacturer's processing software, *RIEGL* RiPROCESS, was used. For the refraction correction of the LiDAR data, the OPALS module Snellius was used with 1.3355 as the refractive index of water (Parrish, 2020; Mobley, 2010; Austin & Halikas, 1976).

A local GNSS base station was set up in the study area to allow preliminary geo-referencing of the ALB data. However, to provide the best possible transformation between the ALB data and the RTS, and

https://doi.org/10.58440/ihr-31-2-a14

thus MBES, data we used reference planes to indirectly geo-reference the ALB data by aligning the ALB data with the RTS-measured planes and eliminating the remaining datum shift. The workflow for indirect geo-referencing of the ALB data is illustrated in Fig. 4. In addition to planar features available in the study area, six reference planes were set up in our study area, i.e. wooden saddle roofs of 80 cm by 60 cm. For each of these planes at least eight points were measured with RTS. The estimated accuracy of each point, in our local network, is better than 5 mm and each plane is estimated based on a least-squares plane-fit. By performing point sampling on the estimated plane, we obtain a point cloud representation of the RTS-measured planes. In the ALB data, the points which correspond to the planes were manually selected based on the preliminary geo-referencing of the ALB data. Then, the shift relative to the RTS-measured planes is calculated using an Iterative-Closest-Point algorithm which only estimates a translation vector. Thus, the ALB point cloud can be transformed into the local coordinate frame by applying this translation vector. We refer to this as indirect geo-referencing with RTS. The estimated shift is $(-3.7,0.4,-5.7)^T$ cm, which meets the accuracy expectations of GNSS in mountainous environments. We use the ALB data in Section 4.3 to show that we achieve bias-free data sets by using RTS-based (indirect) geo-referencing for ALB and MBES.

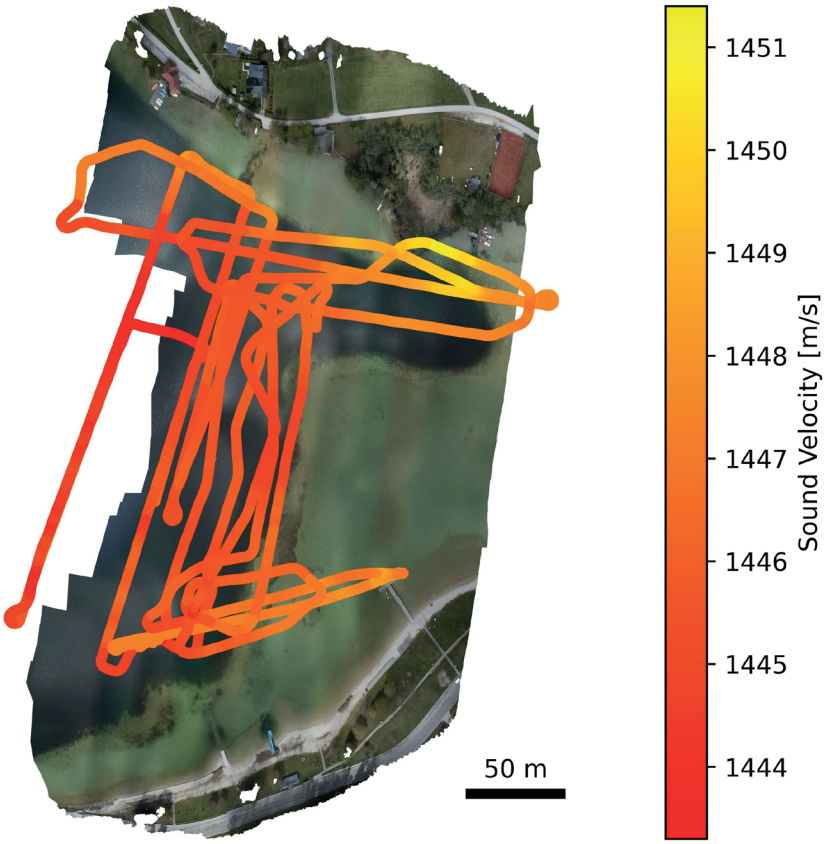


Fig. 3 Map of the measured sound velocities near the water surface by the MBES.

3 Method

In this section, we first describe our two sensor integration approaches for the multi-sensor system consisting of RTS, MBES, and IMU. The first approach uses only the RTS and IMU data for the trajectory estimation, while the second approach additionally leverages planar-correspondences of the MBES data for the trajectory estimation. Afterwards, we investigate the impact of adjustment-based improvements of the trajectory with regard to incorrect sound velocity correction of the MBES data.

In Fig. 5, we show our workflow, together with the software used, to produce the geo-referenced MBES data set. The ALB data are processed entirely in proprietary software and thus omitted from our flowchart.

3.1 Trajectory estimation with RTS/IMU or GNSS/IMU

The determination of platform position and orientation, i.e. trajectory estimation, is framed as a probabilistic parameter estimation problem, where trajectory parameters and mounting calibration are estimated from noisy measurements stemming from the inertial sensors, a positioning sensor (GNSS or RTS), and optionally a mapping sensor (LiDAR or MBES). The use of full-rate IMU measurements and high-fidelity modelling of the trajectory at the same rate leads to a large number of observations and parameters in the adjustment. A recent extension, also employed here, addresses this by introducing an iterated down and upsampling scheme that reduces the number

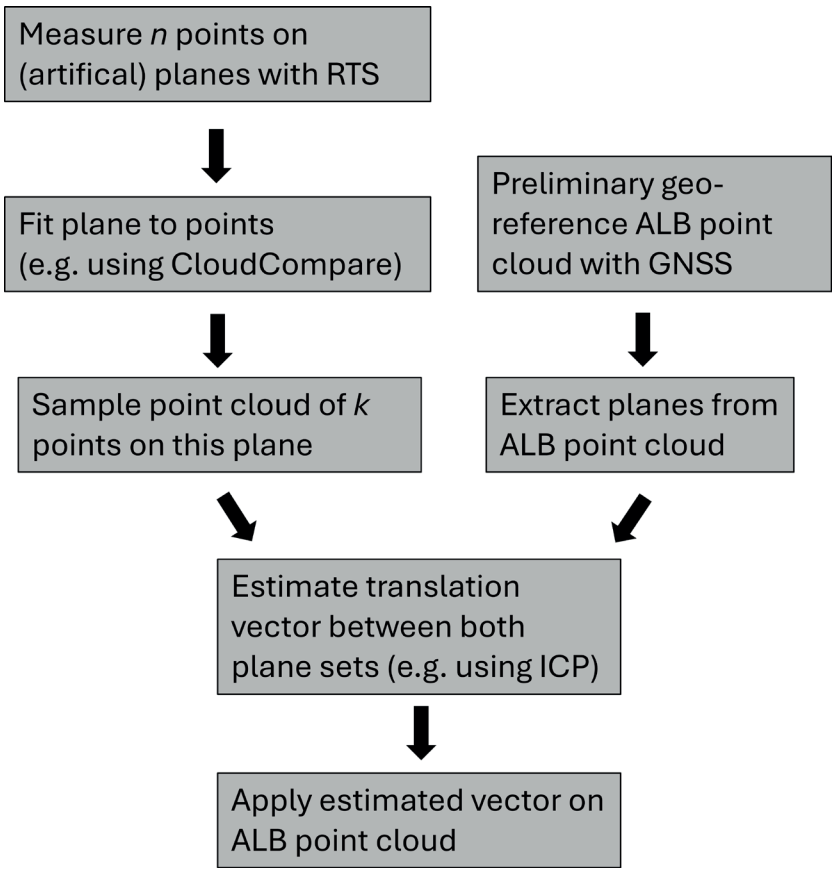


Fig. 4 Flowchart of indirect geo-referencing of ALB data based on RTS measurements.

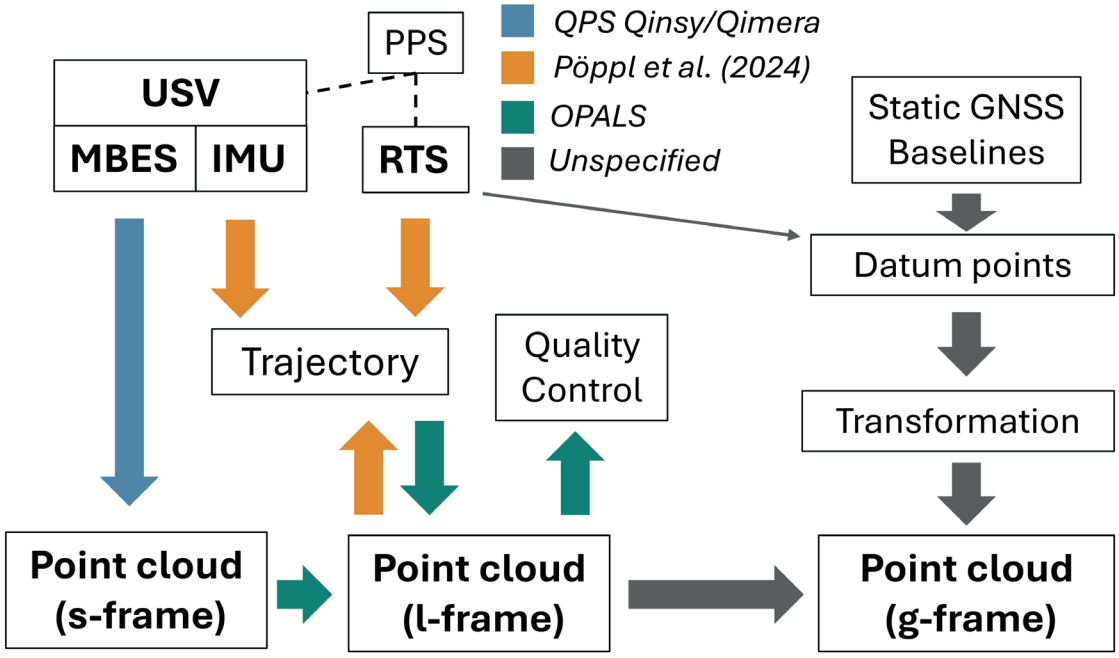


Fig. 5 Flowchart of data processing. Dashed lines represent GNSS timing information (Pulse-Per-Second). S-frame denotes the sensor frame, l-frame the local navigation frame, and g-frame the global frame.

of parameters and measurements in the adjustment while retaining the full frequency spectrum in the trajectory (Pöppl et al., 2025).

The original methodology was designed for ALS applications with GNSS positioning and is here adapted by substituting GNSS with RTS and LiDAR with MBES. Each measurement type is explicitly modelled by Eqs. 1–3. The difference between model and measurement is then minimized in a non-linear least-squares adjustment. All noise is assumed Gaussian with zero-mean, i.e. free from systematic influences, and known covariance. The functional and stochastic models for the inertial measurements remain the same as in previous works (Dammert et al., 2025b; Pöppl et al., 2024). For the GNSS-based direct geo-referencing of the MBES data an adjustment independent from RTS is performed which uses the inertial measurements and GNSS positions. The stochastic model of the GNSS positions is defined by the covariance information derived from the GNSS processing. For our study the GNSS processing yielded estimated standard deviations between 5–15 mm per coordinate component.

Eq. 1 gives the observation equation for the position, where $\tilde{p}$ is the measured position at time t, either from the RTS or from GNSS, $p(t)$ the modelled platform position, $R(t)$ the orientation, and l_a the lever arm of the prism or GNSS antenna respectively. The parameter ϵ_p denotes the gaussian, zero-mean, noise component

$$\tilde{p} = p(t) + R(t) \cdot l_a + \epsilon_p \tag{1}$$

The model of the inertial measurements (Eq. 2) considers the biases $b_f(t)$ and $b_\omega(t)$, the scale factors S_f and S_ω of accelerometers and gyroscopes respectively, which are made up as diag(s_{xf},s_{yf},s_{zf}) and diag($s_{x\omega}$,$s_{y\omega}$,$s_{z\omega}$) respectively, as well as additive white noise ϵ_f and ϵ_ω of the three-axis accelerometer and gyroscope. The obtained measures are the specific force $\tilde{f}$ and the angular velocity $\tilde{\omega}$.

$$\begin{aligned} \tilde{f} &= (I + S_f) \cdot f(t) + b_f(t) + \epsilon_f \\ \tilde{\omega} &= (I + S_\omega) \cdot \omega(t) + b_\omega(t) + \epsilon_\omega \end{aligned} \tag{2}$$

For the trajectory estimation, we use a local north-east-down coordinate system (l-frame), which originates at an arbitrary selected point of our study area. The transformation between this local coordinate system and the global coordinate frame (g-frame), i.e. the reference frame of the GNSS measurements, is estimated from our static GNSS baseline observations. For the RTS-based direct geo-referencing of the MBES data, inertial measurements and RTS positions are included in the adjustment. For simplicity, the measurement equation for RTS is the same as for GNSS, and the integration is done on the coordinate level and not based on polar measurements. For the position measurements derived from the RTS, available as Cartesian coordinates, the covariance information of the RTS is estimated using a Monte-Carlo simulation (Dammert et al., 2025a).

The Euclidean norm of the standard deviation of the horizontal coordinates and the standard deviation of the vertical coordinates based on the simulated distributions of the USV trajectory, derived from RTS measurements, are shown in Fig. 6. Both components show a small variation over the trajectory, ranging less than 1 mm with a median value of 5.6 mm for the Euclidean norm of the horizontal position and 3.7 mm for the vertical position. For the trajectory estimation, we introduce a full covariance

https://doi.org/10.58440/ihr-31-2-a14

matrix extracted from our simulation. Geo-referencing of MBES data is handled using the OPALS software (Pfeifer et al., 2014).

3.2 Trajectory estimation with RTS/IMU/MBES or GNSS/IMU/MBES

In Fig. 7, the general workflow of the multi-sensor adjustment is visualized. A first MBES point cloud is obtained by using a preliminary RTS/IMU trajectory for the geo-referencing. The introduction of MBES data in the adjustment is performed functionally in the same way as for LiDAR data (Pöppl et al., 2024).

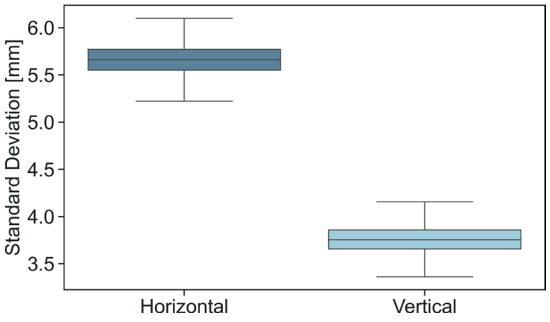


Fig. 6 Simulated standard deviation of all trajectory points measured by RTS. Horizontal refers to the Euclidean norm of the x and y component.

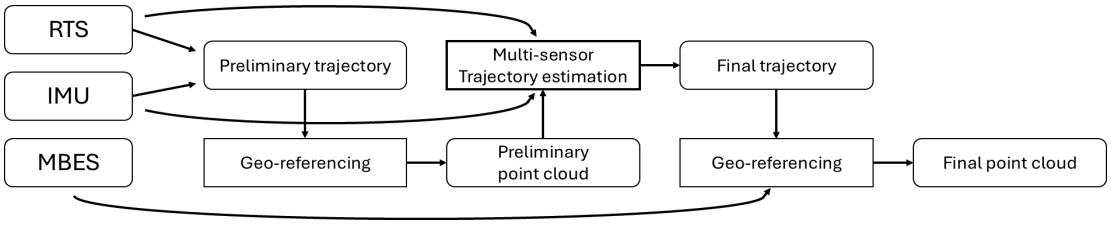


Fig. 7 Trajectory estimation workflow in the multi-sensor trajectory estimation based on RTS, IMU, and MBES.

Based on the preliminary point cloud, the points are sorted in a time-segmented voxel structure (Fig. 8), and a principal component analysis (PCA) is computed for each time segment within each voxel (Fig. 9).

The PCA results are filtered on the basis of planarity conditions, and a best-fit plane, a planar feature or feature plane, is obtained for all remaining voxels.

The corresponding observation Eq. 3 describes the planar features, derived from the MBES point cloud, using the plane centre $\tilde{c}$ and plane normal $\tilde{n}$. Planar features in the same voxel and with similar plane orientation are assumed to correspond to the same planar object. The planar object is then defined by its plane centre c and its plane normal n. Using these definitions, three constraints are defined which describe the normal distance between the planes and the slopes of the object plane with reference to the feature plane axes $\tilde{k}_1$ and $\tilde{k}_2$, which are orthonormal to each other as well as the plane normal n. Here, ϵ_{n,k_1,k_2} denotes again the noise components.

$$
\begin{aligned}
0 &= (c - \tilde{c}) \cdot \tilde{n} + \epsilon_n \\
0 &= \frac{\tilde{n} \cdot \tilde{k}_1}{n \cdot \tilde{n}} + \epsilon_{k_1} \\
0 &= \frac{\tilde{n} \cdot \tilde{k}_2}{n \cdot \tilde{n}} + \epsilon_{k_2}
\end{aligned}
\tag{3}
$$

Planes within the same voxel but different time segments are matched and merged into one object plane (Fig. 9). Correspondences between feature planes and object planes are formed, which in turn are introduced in the adjustment as three observations (Eq. 3): the normal distance and the slope with respect to both plane axes. The object planes are modelled explicitly, with

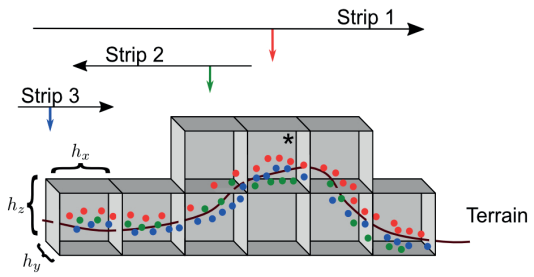


Fig. 8 Points are voxelized and clustered by time (Pöppl et al., 2024).

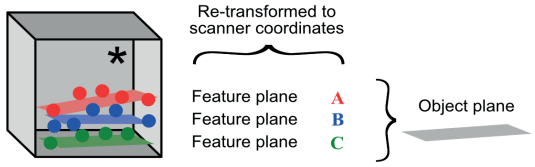


Fig. 9 For each voxel and time-cluster, a PCA is computed. All feature planes belonging to a single cell are combined into a corresponding object plane (Pöppl et al., 2024).

three parameters per plane. Note that the core adjustment is the same as in the previous section, with the only difference that a new class of observations is added: the MBES-derived plane observations. Thus, the multi-sensor adjustment yields an improved trajectory estimate by minimizing discrepancies in the point cloud data. For the stochastic model of the MBES measurements, we rely on the manufacturer's data sheet, which states a range resolution of about 10 mm (Norbit Subsea, 2021). In the absence of any uncertainty specifications, we treat the range solution as standard deviation of the distance

measurement. However, we tested different values for this distance uncertainty and found the effect on the estimated trajectory to be smaller than 2–3 mm and thus neglectable.

Although the measurement equations and the feature extraction and matching process are the same as for the LiDAR case, the extraction parameters have to be adapted to account for the different point density, error characteristics, and environment geometry in MBES data. Voxel size and time segment length must be chosen so that sufficient points are available for a plane-fit within each voxel and time segment. A large voxel size is generally more robust as more points are available for the PCA within each cell but may result in decreased precision as the fidelity of the plane model decreases because the assumption of planarity is generally violated at larger scales. On the other hand, a small voxel size enables better plane approximations for smaller features in the environment geometry but may result in a large amount of spurious correspondences. Additionally, a small voxel size results in a large number of observations in the adjustment and thus require computational effort to solve the adjustment problem or additional filtering of planes. Thus, the choice of voxel size is generally a trade-off between precision of the plane model, robustness of correspondences and computational effort. Here, a voxel size of 1 m and a maximum time segment length of 3 s are used. The time segment was selected to allow the separation of different survey strips, while, as stated in Pöppl et al. (2024), including at least two voxels even for the slower parts of our survey. In the final step of the multi-sensor adjustment, the original MBES data, in the s-frame, is geo-referenced using the final trajectory (Fig. 7).

3.3 Impact of small orientation changes on sound velocity correction

The optimization of bathymetric MBES data holds a key challenge. The range and refraction correction, necessary to compensate for the transition between different layers of the water column, is usually applied to the initial geo-referenced data. After estimation of an improved trajectory, ideally the uncorrected measurements would be used and the sound velocity correction re-computed based on the new trajectory. However, for our study, the uncorrected measurements are not available, therefore, we estimate the error exhibited by not re-computing the sound velocity correction. For our data set, our pre-investigation reveals that the resulting error caused by neglecting this re-application of the refraction correction is smaller than our expected measurement noise. To demonstrate this, we assume a sound velocity profile with constant gradient g, and use the corresponding equation to calculate the measured depth z given in (IHO, 2005):

$$z = \int_0^{\frac{\Delta t}{2}} (c_0 + g \cdot z) \cdot \cos(\theta)\, dt \qquad (4)$$

We use the measured surface sound velocity c_0 of 1445 ms^{-1}, and the measured sound velocity gradient g of about 1 s^{-1}. We perform our calculation for beam angles θ between 0° and 75°, and a signal one-way run time $\Delta t/2$ between 4 ms and 16 ms, depending on the beam angle, which corresponds to a constant water depth of approximately 6 m, which is the average water depth of our study area. To assess the impact of an improved boresight misalignment or vessel orientation on the calculated depth value, we vary the beam emission angles by steps of 0.1° between 0° and 0.5°. Improvements of the vessel position do not have a significant impact on the necessary correction of sound velocity. Horizontal shifts of the position have no effect, if we can assume practically identical sound velocity profiles in the range of the position shift, which is usually in the range of a few cm. A vertical shift of the platform would also shift the application point of the sound velocity profile and thus shift the vertical coordinate of the water bottom measurement itself but not affect the applied correction which is relative to the MBES. The estimation of varied beam emission angles is shown in Fig. 10.

We can conclude that, for near-nadir soundings, the effect on the depth measurement is negligible, independent of the variation of the beam angle. However, for soundings with larger beam angles, e.g. a beam angle of 45°, a change in MBES orientation of 0.5° leads to a 6 cm different depth. For small changes of less than 0.1°, the deviation of about 1 cm is smaller and below the measurement uncertainty of the MBES. Thus, the error introduced by relying on the initial sound velocity correction of the acquisition software increases with the beam angle and the variation of the sensor orientation. In general, this means that we need to include the sound velocity correction in the multi-sensor adjustment when processing acoustic data. However, for the study at hand, we see that the rotation deviations between the initial trajectory and the trajectory estimated in the multi-sensor adjustment are below 0.06°. When separating the different angles, the yaw angle shows the largest differences, while the pitch and roll differences are smaller than 0.01°. In addition, the estimated improvement of the boresight misalignment shows values below 0.05°. Consequently, the change of rotations is smaller than 0.11°. Thus, with reference to Fig. 10, we conclude that the error introduced due to not re-applying the sound velocity corrections is smaller than 1 cm, for soundings with beam angles less than 45°, and therefore acceptable.

4 Results

In this Section, we first analyse our RTS-based MBES data set, resulting from the multi-sensor adjustment. In Section 4.1 we analyse the height discrepancies, i.e. precision, in the overlap areas of the MBES data. For this we compare the precision values from direct geo-referencing and after the multi-sensor adjustment and show the improvement achieved through

https://doi.org/10.58440/ihr-31-2-a14

the multi-sensor adjustment. We also focus on the effect of different swath widths on the precision.

Afterwards, in Section 4.2, we compare the RTS-based data set to the GNSS-based data set using the trajectory residuals of the adjustment, the final trajectory differences, and the resulting precision of the RTS- and GNSS-based data sets after direct geo-referencing and after multi-sensor adjustment. These comparisons show the improvement that the RTS-based data set allows compared to the GNSS-based data set. Finally, in Section 4.3, we compare the MBES data, geo-referenced by RTS, to the ALB data, indirectly geo-referenced by RTS with the reference planes. The comparison is performed first in a quantitative comparison that shows the height differences between both data sets. This is followed by a qualitative comparison that focuses on the characteristics of both data sets.

While we can conduct the latter comparison in the l-frame, the comparison of the RTS-based data set to the GNSS-based data set is done in the g-frame. This introduces the transformation uncertainty, based on the static GNSS baselines, in our results.

For all point cloud processing and raster operations described in this Section we use the scientific point cloud processing software OPALS (Pfeifer et al., 2014).

4.1 RTS-based MBES data

For the relative evaluation of the geo-referencing quality of our data sets, we rely on the Quality package of OPALS described in Ressl et al. (2008). We focus on the precision of the directly geo-referenced data set and the data set resulting from the multi-sensor adjustment. For quality evaluation, each strip is converted into a digital elevation model (DEM) using a grid size of 20 cm and moving planes interpolation. The overlaps of all strips, using a swath width of 90°, are determined. Especially in the shallower part of Lake Erlauf we have very little overlap between the different strips in our data set (Fig. 1). Thus, the precision can mostly be calculated for the deeper sections of the study area. After matching the strips into pairs, the DEM of Difference (DoD) model is calculated for each overlapping strip pair.

4.1.1 Precision of RTS-based MBES data

Fig. 11 shows the aggregated differences of the DoDs of all 84 strip pairs after direct geo-referencing using the RTS/IMU integration (left) and after multi-sensor adjustment (right). It shows that the change in the mean value is negligible and that both distributions are roughly cantered around 7 mm to 8 mm. However, the standard deviation of the differences is reduced by 33 % after multi-sensor adjustment. Most importantly, the number of values that exceed the range from -10 cm to 10 cm (orange overflow bins) reduces from 6 % to 2 %. Consequently, the multi-sensor adjusted data set shows the expected outcome of increased precision of the data due to the consideration of the MBES information.

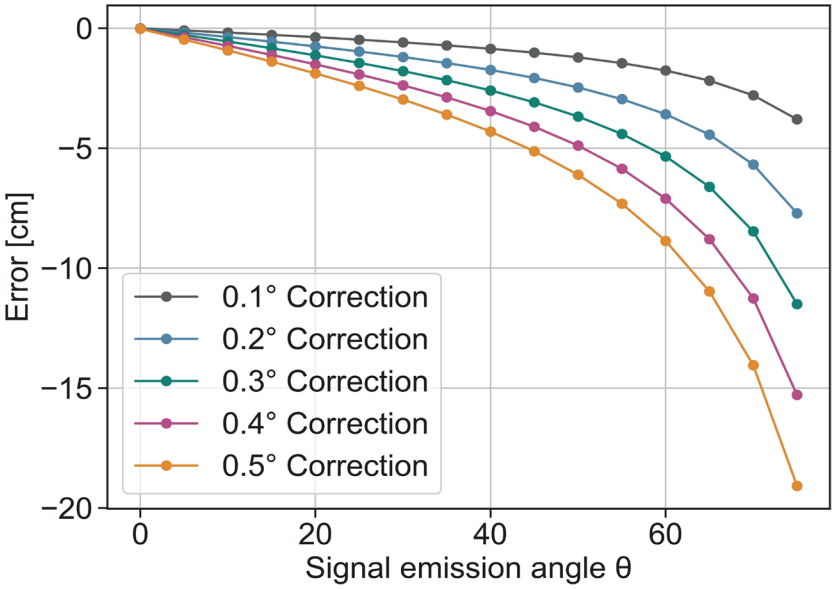


Fig. 10 Effect of varying orientation or beam emission angles on the sound velocity correction.

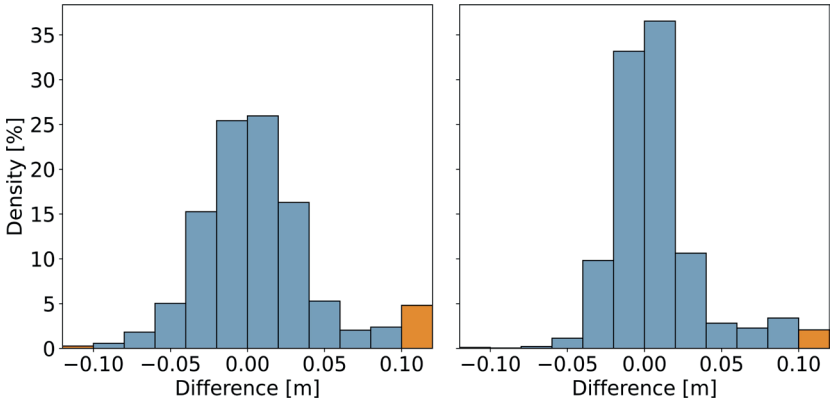


Fig. 11 Histogram of the height precision of RTS/IMU integration (left) and multi-sensor adjustment (right). Orange bins sum up all values that exceed -0.1 or 0.1 m respectively.

4.1.2 Effect of swath width

Due to the larger impacts of orientation uncertainties, sound correction uncertainties and, in general, a longer interaction with the water column, the outer beams of a swath are less accurate than the inner beams. In Lucieer et al. (2016), the increasing uncertainty of multibeam systems with increasing distance to the nadir beam is investigated on the basis of simulations. In (Grzadziel & Waz, 2016), experiments are carried out and a swath width of 90° is recommended as the most effective swath width. Thus, we focus on data with a swath width of 90° but also investigate the effect of different swath widths on the resulting precision. However, we only limit the swath width in post-processing. Fig. 12 shows the distribution of the precision of all strip pairs after the multi-sensor adjustment for increasing swath widths ranging from 30° to 180°. The figure shows the mean and median values, as well as the 60th, 70th, 80th, and 90th percentiles.

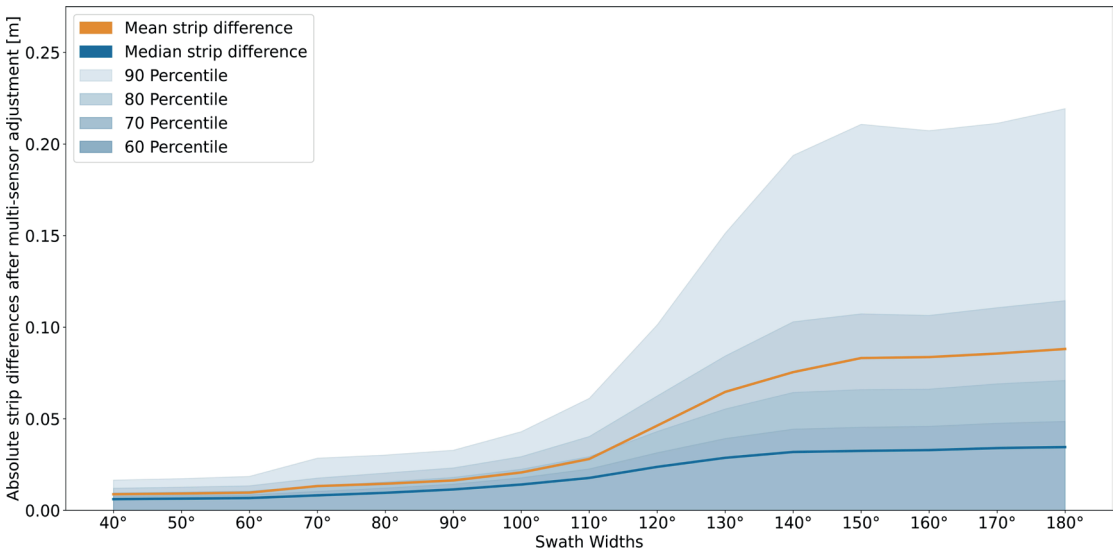


Fig. 12 Distribution of the precision (i.e. height differences) over all strip pairs for increasing swath widths after multi-sensor adjustment.

In general, we see a decrease in the exhibited precision with increasing swath widths. Regarding the best possible precision, we can conclude that a swath width smaller than 60° provides the best results, as the narrow beams of an MBES are generally more accurate than the outer beams. While many factors contribute to the lower accuracy of the outer beams, e.g., footprint size, signal attenuation and incidence angle, the inaccurate SVP used in our study also has, due to the longer interaction time of the signal with the water column, a large effect on the precision for larger swath widths. Consequently, a narrow swath width of 60° might be most useful when performing multibeam surveys aiming at highest accuracy. At a swath width larger than 100° we see an amplification of the increase of the point cloud discrepancies. However, it is worth noting that these particular values depend on the specific data set, e.g., water body, availability of sound velocity data, and MBES system. For our data set it is reasonable to use a swath width of 90° as compromise between accuracy and efficiency / strip overlap as a swath width of 60° would lead to an insufficient overlap for our investigation. These results should be especially interpreted in the context of the different sound velocities shown in Fig. 3, as our imprecise sound velocity profile leads to these large discrepancies in the outer swath areas.

4.2 Comparison of RTS- and GNSS-based data set

In this subsection, we compare our RTS-based data set with the GNSS-based data set for the areas where both are available (Patches 1–3). Both data sets follow the same processing workflow (Sections 3.1 and 3.2) and are thus comparable. We first focus on the exhibited residuals of the (multi-sensor) trajectory estimation process and then compare the resulting trajectories directly. Afterwards, we compare the precision exhibited by both data sets.

4.2.1 Residuals of trajectory estimation

Fig. 13 shows the residuals of the trajectory estimation as part of the multi-sensor adjustment. When analysing those residuals, we see that the Euclidean norm of the horizontal trajectory component of the RTS- and GNSS-based data is quite similar with median values of 2 mm and 4 mm, respectively. The interquartile range (IQR) shows a spread of 2 mm (RTS) and 3 mm (GNSS). As the horizontal component is given as the Euclidean norm of the along- and across-trajectory component, a median value of zero is not expected. The vertical component exhibits a strong difference for both data sets. While the RTS data show a median of 0 mm with an IQR of less than 1 mm, the GNSS data show a median of 0 mm with an IQR of 12 mm. Thus, while the horizontal residuals are quite similar with the RTS showing slightly smaller residuals than the GNSS, the vertical residuals are more than ten times smaller for the RTS data set. It should be noted that, while the residuals show the agreement between the three subsystems (RTS or GNSS, IMU, and MBES) considered in the multi-sensor adjustment, they do not reflect the absolute accuracy of the trajectory, because the absolute positioning system (RTS or GNSS) has no redundancy.

4.2.2 Trajectory comparison of RTS- and GNSS-based trajectory estimation

Fig. 14 shows the horizontal (Euclidean distance) and vertical discrepancies of the trajectory estimates based on RTS and GNSS of the position part of the trajectory for the data Patch 3. For the calculation of the absolute trajectory errors, we use the trajectory evaluation package *trajectopy* (Tombrink et al., 2024). The horizontal differences (Euclidean distance) show strongly varying values that range up to 8 cm with a mean value of about 3 cm. However, the average deviations of x and y are close to zero. The vertical

https://doi.org/10.58440/ihr-31-2-a14

component shows a similar strong variation with an overall upward trend but has a mean value close to zero. Based on the adjustment residuals and theoretical knowledge of the height accuracy of both RTS and GNSS measurements, we can allocate the vertical discrepancies largely to the accuracy of the GNSS measurement.

4.2.3 Comparison of precision

We also compare the precision for the RTS-based data (Section 4.1.1) with the differences obtained from the analogue GNSS processing. These results are shown in Fig. 15 for both steps, RTS/IMU-based direct geo-referencing and multi-sensor adjustment. There, the precision over all 84 evaluated strip pairs is aggregated and shown as box plots. First of all, we see a higher variation of the precision for the directly geo-referenced data sets, which is in agreement with Fig. 11. For those directly geo-referenced data sets, we see a larger variation for the GNSS data than for the RTS data. Regarding the IQR, GNSS achieves a value of 12 cm and RTS of 8 cm. After performing the multi-sensor adjustment, both distributions are similar with an IQR of 4 cm, showing the large weight of the MBES observations in the adjustment process. Note that the precision does only show the relative agreement between the survey strips, and the similar IQR values of GNSS and RTS after the multi-sensor adjustment does not mean that both data sets have a similar accuracy. However, we observe that the GNSS-based data set shows approximately 50 % worse precision than the RTS-based data set for directly geo-referenced data sets.

4.3 Differences between MBES and bathymetric LiDAR

For comparison between MBES and ALB, we use the final MBES data sets resulting from multi-sensor adjustment based on RTS. Due to the adjustment, the effects of lever arm and boresight misalignment errors are minimized, and, due to the RTS-based geo-referencing of the MBES data and indirect geo-referencing of the ALB data with reference planes, the impact of geo-referencing uncertainty is reduced for both data sets. This approach enables a comparison of both techniques that focusses on the sensors (MBES and ALB) themselves and minimizes the impact of the geo-referencing uncertainty. Due to the lack of reference data in our study, we use this comparison as quality assessment. For our comparison, we use the overlap region of the RTS-based MBES and ALB data (Fig. 1, Patch 1).

It is important to note that, in our study, neither of the techniques can be regarded as reference for the other as we assume both techniques to have similar accuracy values. Consequently, this comparison shows the agreement of both techniques and should serve as motivation for future work where, (i) both techniques can be compared based on reliable reference data or (ii) the integration of MBES and ALB data can be improved by use of the hardware- and software-based approaches presented in our study.

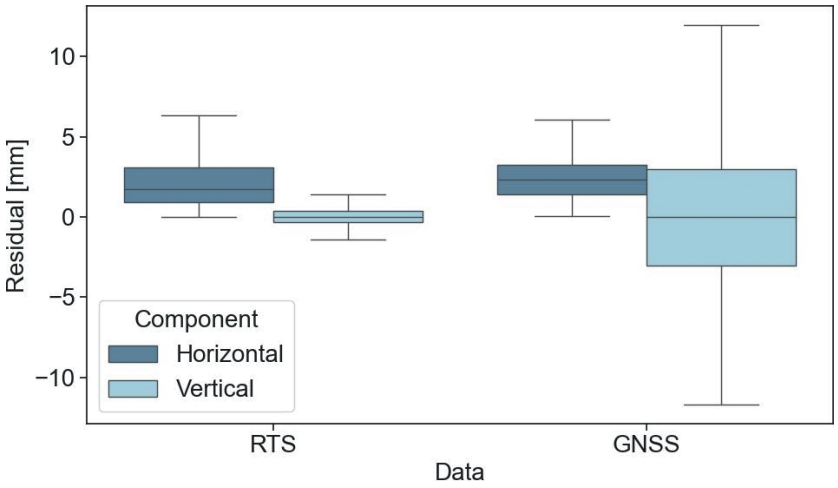


Fig. 13 Residuals of the multi-sensor adjustment combined over all RTS data patches.

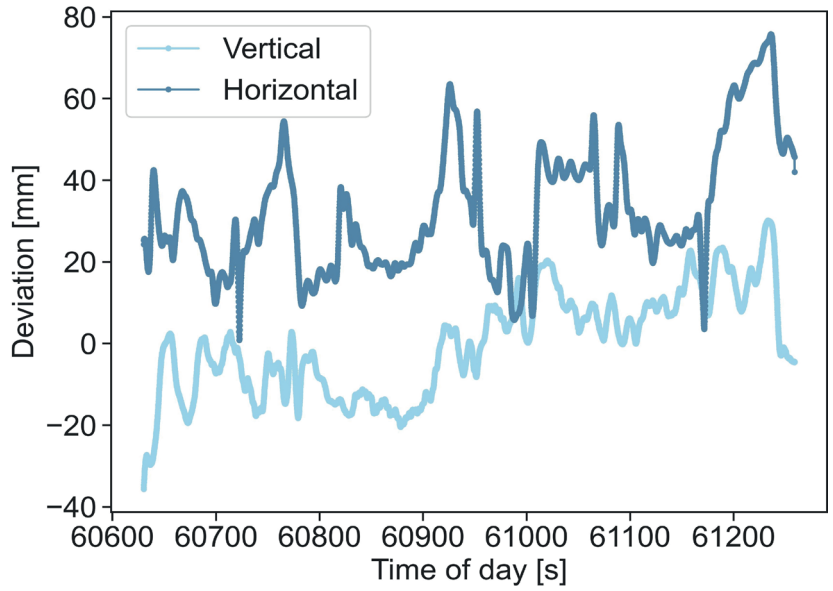


Fig. 14 Discrepancies between RTS- and GNSS-based trajectory estimates.

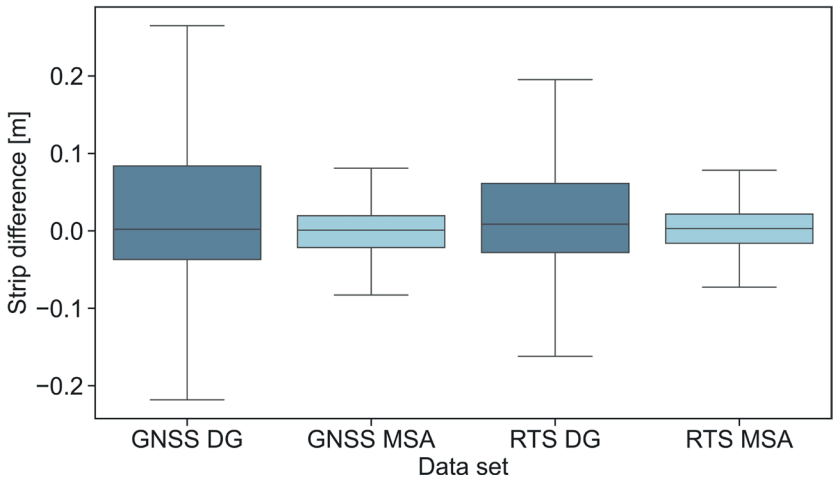


Fig. 15 Precision of all strip pairs for RTS and GNSS data sets, after direct geo-referencing (DG), and after multi-sensor adjustment (MSA).

4.3.1 Quantitative comparison

We compute a DoD grid model for the comparison of both data sets. Both DEMs that serve as input, represent the combined point clouds of the MBES and ALB data, respectively, considering all acquired strips. For the gridding of the point clouds, we use moving planes interpolation and a grid size of 0.5 m. We found the grid size of 0.5 m to allow for robust results that show an acceptable noise level while still giving a high spatial resolution. To allow a reliable comparison of both DEMs, we exclude cells with a point density lower than 15 points per m², which corresponds to the 2.5th percentile of the point density of the ALB data, for the ALB and MBES data. We do this to exclude areas which show incomplete coverage, e.g. because they are too deep for the ALB to penetrate.

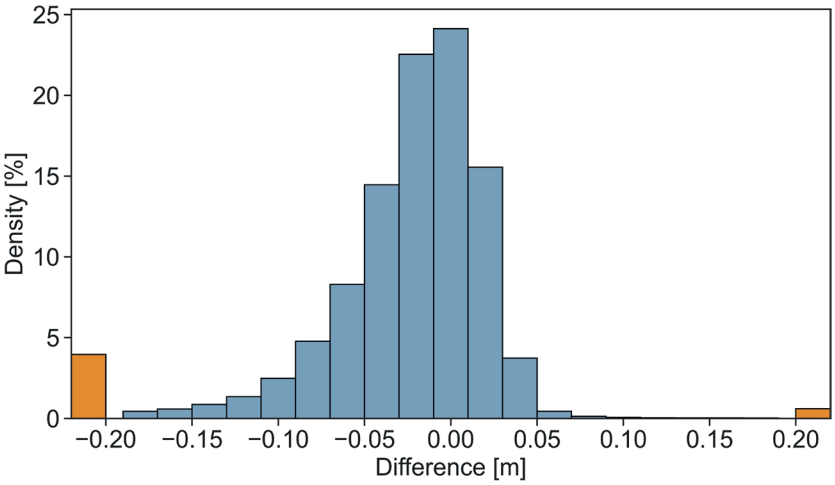


Fig. 16 Histogram of the computed differences between RTS-based MBES data and ALB. Orange bins sum up all values that exceed -0.2 or 0.2 m, respectively.

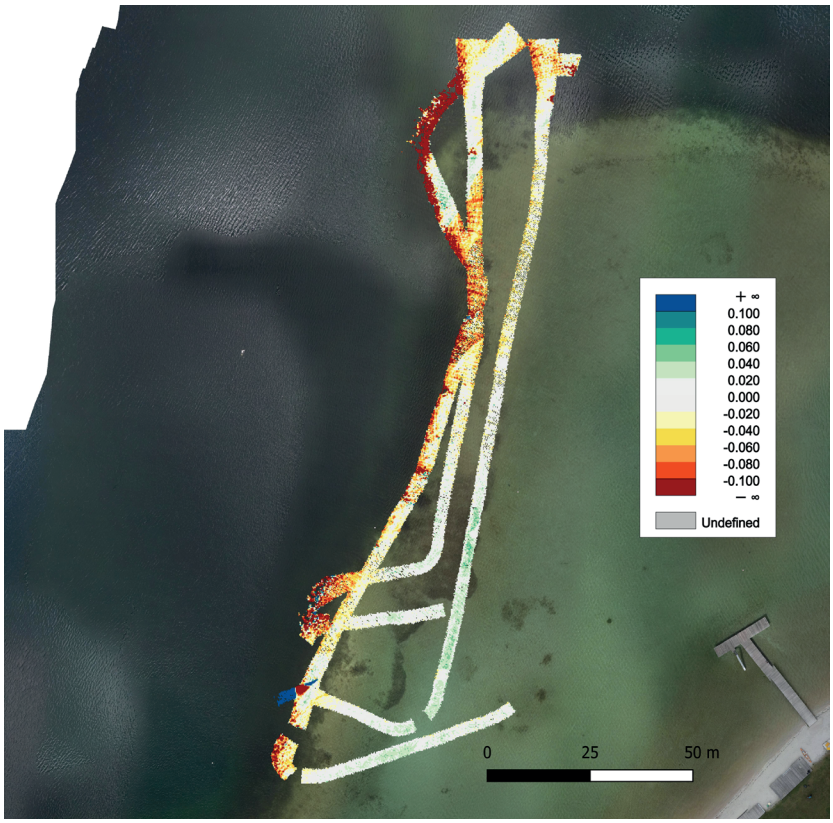


Fig. 17 Map of the differences between RTS-based MBES data and ALB.

Figs. 16 and 17 show the differences between the ALB and the MBES data set as a histogram and as a map visualization. The distribution of the differences shows a slightly asymmetrical shape with a negative centre and a mean value of -2.1 cm. The median value is -1.4 cm and the standard deviation is 4 cm. The asymmetric shape of the histogram is also represented by the percentiles, which show that 75 % of the differences are smaller than 5 mm and 95 % are smaller than 2.5 cm. We clearly see that the ALB measures lower height values than the MBES. The orange bars in the histogram are outlier boxes, which aggregate all values lower or higher than the value range, i.e. -20 cm and 20 cm. Therefore, the boxes show the share of outlier measurements, which is about 3 %. Together with the map visualization (Fig. 17), we see that outliers occur mainly in the deeper areas of the study site, where the extraction of water bottom points from ALB is hardly possible due to signal attenuation. This fact is then seen in the higher measurement noise. In general, the ALB was able to extract bottom points until 10 m water depth. Additionally, in the central part we see an artifact of negative difference, coloured red, which presumably originates from a single ALB strip being slightly lower than the remaining flight block. Finding the reason for the asymmetry of the differences between ALB and MBES is beyond the scope of this article and will be addressed in our future work. However, possible reasons can be the refraction coefficient, signal processing of the ALB waveforms, or an undetected rotation between the ALB and MBES data.

4.3.2 Qualitative comparison

We also take a closer look at the key differences between the MBES and ALB data sets. The MBES has a smaller footprint and a higher point density resulting in a denser point cloud. For example, the MBES footprint is about 8 cm × 14 cm at 10 m water depth (beam divergence of 0.5° × 0.9°) and the ALB footprint is approximately 20 cm × 20 cm (beam divergence of 0.115°). This is visualized in Fig. 18 (left), where the dense swath of the MBES (blue) and the comparably sparse lines of the ALB (red) are visible. In addition, the larger line spacing of the LiDAR can be seen. However, when considering the platform velocities, MBES about 1 ms^{-1} and ALB about 15 ms^{-1}, the ALB actually exhibits temporally closer lines than the MBES. In Fig. 18 (right), the vertical spread of one strip of MBES and ALB data is shown for a vertical section with a width of 2 m. Although the MBES data are much denser than the ALB data, we see that the vertical spread of the ALB is comparable to or even smaller than the spread of the MBES data. However, similar to Fig. 16, we observe a tendency of the ALB data to be lower than the MBES data.

https://doi.org/10.58440/ihr-31-2-a14

5 Discussion

When discussing the use of RTS for trajectory estimation of kinematic multi-sensor systems it is important to keep the limitations in mind. First of all, the RTS relies on an unobscured line-of-sight towards the target. Secondly, the range of the automated target tracking is limited. The threshold value depends on the weather, e.g., rain, mist or certain sunlight conditions reduce the achievable range, and on the prism. In our tests, we found a range of 800 m to be a conservative and reliable estimate for the range threshold when tracking fast moving targets, e.g., airborne drones. In the context of bathymetry, where speeds are often lower than for airborne platforms, the target tracking, at least of the modern RTS models, is very robust. The lower speed also allows to re-establish the target tracking on-the-fly if the target tracking fails, e.g. due to a line-of-sight interruption. In terms of trajectory estimation, those short measurement gaps can be regarded similar to GNSS outages that appear e.g. under bridges. Those short gaps can easily be bridged by the relative position information of the IMU. The limited range of RTS restricts our proposed RTS-based trajectory estimation to inland waters, harbours, and shorelines. However, these are often the areas where highest accuracy is required and GNSS signal obstructions usually occur, e.g. by quay walls.

In general, our contribution shows two separate approaches to improve the overall quality of hydrographic data: (i) the application of RTS for more accurate trajectory measurements, which is a hardware-based approach, and (ii) the multi-sensor adjustment making use of all available information during the trajectory estimation, which is a software-based approach. While (i) is limited to inland and coastal waters that allow the tracking and measurement of the target platform from a shore-based RTS, (ii) is applicable for inland and maritime waters. The main limitations for (i) are thus the limited range of about 800 m and the requirement to be able to set up an RTS. On the other hand, (ii) requires position (RTS or GNSS) and IMU data together with an MBES or LiDAR point cloud and stochastic information for all input data. Thus, it is applicable on most bathymetric data sets. However, (i) allows accurate trajectory information with accuracies in the sub-cm level leading to a potentially very accurate bathymetric point cloud. The multi-sensor adjustment (ii) is limited by its input data. Thus, without accurate trajectory or reference data the resulting point cloud might be precise, i.e. show little discrepancies, but have a lower accuracy. While (i) and (ii) complement each other very well, both approaches can be used independently to improve the quality of bathymetric data.

For our data set, the multi-sensor adjustment excels at creating consistent data. We see a decrease in the strip differences by 33 % when processing our data set with the multi-sensor adjustment, since the point cloud information is used to minimize the discrepancies. The results highlight the importance of integrated, multi-sensor processing strategies in obtaining high-precision data sets. However, such processing strategies are unable to detect systematic shifts of the data, e.g. due to geo-referencing uncertainties, without the use of additional information such as reference geometries. Thus, it works well alongside sensors such as RTS, which are used to determine accurate, absolute trajectories, to obtain a data set with high precision and accuracy.

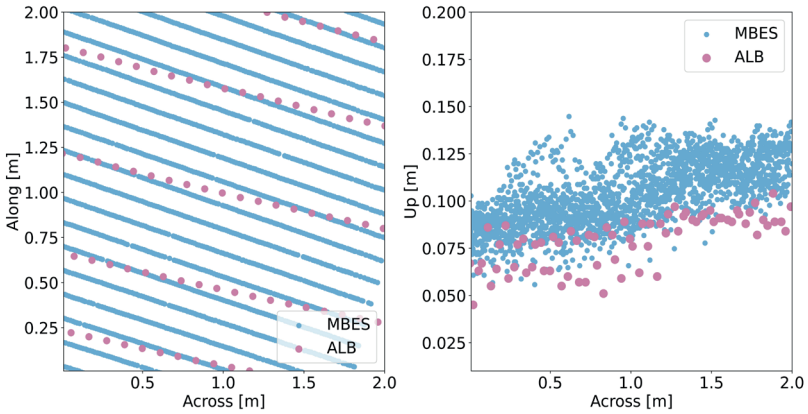


Fig. 18 Characteristics of MBES and ALB: Horizontal plane (left), vertical cross section (right).

However, while for data on dry land, the multi-sensor adjustment leverages the abundance of different exhibitions of man-made features or planar objects in the point cloud, bathymetric point clouds usually show less distinct features. With the correct parametrization, the planes can be fitted to the water bottom. These planes are mostly horizontal, which does not contribute much regarding the horizontal position of the point cloud. Thus, point-cloud-correspondence-driven approaches can be expected to perform worse for bathymetric point clouds than for topographic point clouds due to the less diverse exposition of planar features. This is one of the reasons, why our study shows the large value of employing both, RTS-based trajectory estimation and the multi-sensor adjustment of the entire data, to generate a data set with high precision and accuracy.

For the RTS-based data set, the residuals of the multi-sensor trajectory adjustment show only slightly better values for the horizontal component compared to the GNSS-based data set. In contrast, the vertical residuals are more than 10-times smaller for the RTS data. This shows overall, the superior accuracy of the RTS-based trajectory compared to the GNSS-based trajectory.

However, the residuals only show relative discrepancies between the measurements of RTS or GNSS, IMU, and MBES. The horizontal coordinates of the RTS and GNSS trajectories, on the other hand, show much larger deviations. Although the horizontal residuals of the multi-sensor adjustment suggest only low discrepancies between the RTS and GNSS-based trajectories, the direct comparison of the RTS and GNSS-based trajectories reveal horizontal and vertical discrepancies at the cm-level. However, without

a reliable reference, those discrepancies cannot be attributed to either of the sensor systems. But the known uncertainty information of GNSS and RTS suggests that the main influence comes from GNSS. Thus, the small horizontal residuals of GNSS can be explained by the high temporal correlation of systematic GNSS errors (Luo et al., 2019; Wang et al., 2022) that are not detected in the trajectory estimation but cause a systematic absolute displacement of the point cloud. This systematic displacement can then be seen in comparison with the RTS data. However, for detailed investigations of the accuracy of GNSS and RTS, topographic airborne LiDAR should be preferred (Dammert et al., 2025b) as the uncertainty introduced by the water column is avoided and reliable reference data are easier to acquire. A detailed discussion of those influences is outside the scope of this work. However, it is worth mentioning that the simulated standard deviations for RTS (Section 3.1) fit well with the residuals shown for the multi-sensor adjustment based on RTS.

By analysing the precision of RTS- and GNSS-based data sets, we can see that RTS-based direct geo-referencing leads to better precision of the multi-sensor system. However, in terms of precision, the added value of the RTS is reduced when data of the mapping sensor or correspondences of the point cloud are included in a multi-sensor adjustment. We assume that the strong similarity between both adjusted data sets (RTS- and GNSS-based) is largely due to the range precision of the MBES. With a ranging resolution of 10 mm (Norbit Subsea, 2021), which we treat as standard deviation due to the lack of any information on the systems accuracy, the MBES range measurements receive a high weight in the least-squares adjustment, leading to a large dependence of the trajectory on the MBES data and a comparably lower weight of the RTS or GNSS data. While we generally assume the RTS positions to have a standard deviation of 3–6 mm, the GNSS positions receive estimated standard deviations from the GNSS processing software. For this study these values range between 5–15 mm. We are aware that these values can be very optimistic, but we do not want to change these values by applying an arbitrary factor to it.

The differences between MBES and ALB show a slight underestimation of the bathymetric height by the ALB relative to the MBES data. Due to the asymmetrical shape of the distribution of differences (Fig. 16) and its median value of -1.4 cm, we can state that there is no height bias, that exceeds the measurement noise of either system, between both data sets. However, the systematic overestimation of the water depth by the ALB data set compared to MBES can originate from various sources. Possible reasons include the different sediment penetration characteristics of both systems (Gaida et al., 2020), the signal processing strategy of the ALB software, a poorly determined water surface (Mandlburger et al., 2013), and an imprecise refraction coefficient used for ALB data processing. We used a refraction coefficient of 1.3355 based on the work of Parrish (2020); Mobley (2010); Austin & Halikas (1976) and observations of water parameters on site. However, the differences between ALB and MBES might as well originate from the processing of the MBES data. Nevertheless, we see that, by applying profound (indirect) geo-referencing approaches such as RTS, the standard deviation of the differences between both systems range is about 4 cm. This magnitude motivates further investigation of the uncertainty budget of the sensors (MBES and ALB). Such an investigation also requires adequate ground truth, a topic which we will address in future work. In our future work we also plan to address the seamless integration of MBES and ALB based on RTS, as well as based on a combined multi-sensor adjustment that leverages point cloud correspondences between MBES and ALB data to create a consistent data set that shows minimized discrepancies in the transition zones between MBES and ALB.

6 Conclusion

In our contribution, we present a workflow for RTS-based geo-referencing of a hydrographic multi-sensor system as basis for a multi-sensor-adjustment-based trajectory estimation that leverages correspondences in the bathymetric point cloud. We present a data set acquired at Lake Erlauf consisting of MBES and ALB data. We use this data set to demonstrate our geo-referencing strategy as well as our quality assessment workflow, based on height discrepancies in the point cloud as measure of the precision. We also investigate the impact of varying swath widths on the precision. The dominant decrease in the precision is seen for swath widths of more than 100°, which allows us to use a swath width of 90° and thus make use of a good overlap in our data. However, we assume that this sharp decrease in precision at larger swath widths is mainly caused by the heterogeneous sound velocity at our study site. The quality of the multi-sensor system's trajectory estimation is evaluated by comparing the residuals and differences of the estimated trajectories for RTS- and GNSS-based processing. Additionally, the influence of the presented trajectory estimations based on deviations in the MBES point cloud is analysed. We also compare the resulting MBES point cloud with the ALB data, where we rely on reference planes to precisely register the ALB point cloud data on the RTS measurements and thus the RTS-based MBES data.

The comparison of RTS- and GNSS-based processing show that using RTS enables more accurate geo-referencing, yielding about ten times smaller height residuals in the estimation process. Also, the GNSS-based data show about 50 % worse precision in the resulting point cloud compared to our RTS-based data. However, by leveraging the MBES data in the trajectory estimation in

https://doi.org/10.58440/ihr-31-2-a14

our multi-sensor adjustment, the precision increases to the same level for both geo-referencing sensors. This large improvement can be contributed to the high weight of the MBES observation in the adjustment process. By comparing the resulting point cloud to the ALB data, we can show that the RTS-based data set exhibits a close-to-zero-centred distribution of vertical differences which shows no remaining significant bias.

By introducing accurate geo-referencing of MBES data based on RTS, we lay the basis for improving the integration of MBES and ALB data. The minimization of the geo-referencing errors allows not only the integration but also the comparison of both sensor techniques to one another but also relative to bathymetric reference data. In addition, the accurate registration of both data sets allows the improved combination of both techniques for seamless data transition and connection in shallow water regions.

Acknowledgments

The authors thank BOKU University and VERBUND AG, who performed the MBES data acquisition, *RIEGL* Laser Measurement Systems, who acquired the bathymetric LiDAR data, MacArtney Germany and QPS, who provided a license for QPS Qimera to allow data processing of the MBES data, and lastly Wolfang Sombrowski from MacArtney Germany for counseling during data processing. This research was conducted within the TrackDrone project (Grant No. 895310) funded by the Austrian Research Promotion Agency (FFG).

References

Austin, R. W. and Halikas, G. (1976). *The index of refraction of seawater* [Technical Report]. UC San Diego: Scripps Institution of Oceanography. https://escholarship.org/uc/item/8px2019m (last accessed 20 July 2025).

Dammert, L., Thalmann, T., Monetti, D., Neuner, H. and Mandlburger, G. (2025a). Numerical simulation and sensitivity analysis of UAS trajectory determination with robotic total stations. *Survey Review*, pp. 1–17. https://doi.org/10.1080/00396265.2025.2517540

Dammert, L., Thalmann, T., Pöppl, F., Monetti, D., Neuner, H.-B. and Mandlburger, G. (2025b). High-precision geo-referencing of UAS data with robotic total stations. *ISPRS Annals of the Photogrammetry, Remote Sensing and Spatial Information Sciences, X-G-2025*, pp. 213–220. https://doi.org/10.5194/isprs-annals-X-G-2025-213-2025

Ernstsen, V. B., Noormets, R., Hebbeln, D., Bartholomä, A. and Flemming, B. W. (2006). Precision of high-resolution multibeam echo sounding coupled with high-accuracy positioning in a shallow water coastal environment. *Geo-Marine Letters 26*(3), pp. 141–149. https://doi.org/10.1007/s00367-006-0025-3

Gaida T. C., Mohammadloo T. H., Snellen M. and Simons D. G. (2020). Mapping the Seabed and Shallow Subsurface with Multi-Frequency Multibeam Echosounders. *Remote Sensing 12*(1):52. https://doi.org/10.3390/rs12010052

Gong, X., Zhang, R. and Fang, J. (2013). Application of unscented R-T-S smoothing on INS/GPS integration system post processing for airborne earth observation. *Measurement, 46*(3), pp. 1074–1083. https://doi.org/10.1016/j.measurement.2012.11.028

Groves, P. (2013). *Principles of GNSS, inertial, and multisensor integrated navigation systems*. Artech house. Norwood, MA, USA.

Grzadziel, A. and Waz, M. (2016). Estimation of effective swath width for dual-head MBES. *Annual of Navigation, 23*, pp. 173–183. https://doi.org/10.1515/aon-2016-0012

Gueriot, D., Chedru, J., Daniel, S. and Maillard, E. (2000). The patch test: a comprehensive calibration tool for multibeam echosounders. *Proceedings of OCEANS 2000 MTS/IEEE Conference and Exhibition, Cat. No.00CH37158*, Providence, RI, USA, 3, pp. 1655–1661. https://doi.org/10.1109/OCEANS.2000.882178

Hesse, C., Holste, K., Neumann, I., Esser, R. and Geist, M. (2021). 3D HydroMapper–Ein innovatives Messsystem für die Erfassung, Prüfung und das Management von Wasser-Infrastrukturbauwerken. *ZfV-Zeitschrift für Geodäsie, Geoinformation und Landmanagement. 4*.

IHO (2005). *Manual on Hydrography* (1st ed.). IHO Publication C-13, International Hydrographic Organization, Monaco. https://iho.int/uploads/user/pubs/cb/c-13/english/C-13_Chapter_1_and_contents.pdf (last accessed 19 October 2025).

IHO (2022). *Standards for Hydrographic Surveys* (6th ed.). IHO Special Publication S-44, International Hydrographic Organization, Monaco. https://iho.int/uploads/user/pubs/standards/s-44/S-44_Edition_6.1.0.pdf (last accessed 19 October 2025).

Kerekes, G. & Schwieger, V. (2018). Kinematic positioning in a real time robotic total station network system. *Proceedings of the 6th International Conference on Machine Control & Guidance,* Berlin, Germany, 1–2 October 2018, pp. 35–43.

Kälin, U., Hürzeler, M. and Grimm, D. (2023). Calibration of Kinematic Measuring Systems. I*ngenieurvermessung 23. Beiträge zum 20. Internationalen Ingenieurvermessungskurs Zürich*, pp. 195–207.

Kälin, U., Staffa, L., Grimm, D. E. and Wendt, A. (2022). Highly Accurate Pose Estimation as a Reference for Autonomous Vehicles in Near-Range Scenarios. *Remote Sensing, 14*(1), pp. 90.

Krzyżek, R., Kudrys, J. (2022). Accuracy of GNSS RTK/NRTK height difference measurement. *Appl Geomat, 14*, 491–499. https://doi.org/10.1007/s12518-022-00450-2

Le Deunf, J., Legris, M. and McManus, J. (2020). Automatic Calibration for MBES Offsets. *Hydro International*. https://www.hydro-international.com/content/article/automatic-calibration-for-mbes-offsets (last accessed 15 July 2025).

Lucieer, V., Huang, Z. and Siwabessy, J. (2016). Analyzing uncertainty in multibeam bathymetric data and the impact on derived seafloor attributes. *Marine Geodesy, 39*(1), pp. 32–52. https://doi.org/10.1080/01490419.2015.1121173

Luo, Y., Li, J., Yu, C., Xu, B., Li, Y., Hsu, L.-T. and El-Sheimy, N. (2019). Research on Time-Correlated Errors Using Allan Variance in a Kalman Filter Applicable to Vector-Tracking-Based GNSS Software-Defined Receiver for Autonomous Ground Vehicle Navigation. *Remote Sensing, 11*(9), 1026. https://doi.org/10.3390/rs11091026

Mandlburger, G., Pfennigbauer, M. and Pfeifer, N. (2013). Analyzing near water surface penetration in laser bathymetry – A case study at the River Pielach. *ISPRS Ann. Photogramm. Remote Sens. Spatial Inf. Sci., II-5/W2*, pp. 175-180. https://doi.org/10.5194/isprsannals-II-5-W2-175-2013

Mandlburger, G., Rhomberg-Kauert, J., Gueguen, L.-A., Mulsow, C., Brezovsky, M., Dammert, L., Haines, J., Glas, S., Himmelsbach, T., Schulte, F., Amon, P., Winiwarter, L., Jutzi, B. and Maas, H.-G. (2025). Mapping shallow inland running waters with UAV-borne photo and laser bathymetry. *Journal of Applied Hydrography, 130*, pp. 42–54. https://doi.org/10.23784/HN130-06

Maxim, A., Lerke, O., Prado, M., Dorstelmann, M., Menges, A. and Schwieger, V. (2017). UAV guidance with robotic total station for architectural fabrication processes. *156. DVW-Seminar Unmanned Aerial Vehicles 2017 (UAV 2017)*, Stuttgart, pp. 145–161. Wißner-Verlag Augsburg.

Mobley, C. D. (2010). Optical properties of water. *Handbook of Optics, 4*, pp. 1–1. McGraw-Hill. New York.

Mokhtar, K., Chuah, L. F., Abdullah, M. A., Oloruntobi, O., Ruslan, S. M. M., Albasher, G., Ali, A. and Akhtar, M. S. (2023). Assessing coastal bathymetry and climate change impacts on coastal ecosystems using Landsat 8 and Sentinel-2 satellite imagery. *Environmental Research, 239* (Part 2/2023), p. 117314. https://doi.org/10.1016/j.envres.2023.117314

Möser, M., Hoffmeister, H., Müller, G., Staiger, R. and Wanninger, L. (2012). *Handbuch Ingenieurgeodaesie: Grundlagen* (4 edn). Wichmann. Berlin.

Norbit Subsea (2021). *Norbit Winghead i77h.*

Parrish, C. (2020). Index of refraction for seawater and freshwater as a function of wavelength and temperature. https://research.engr.oregonstate.edu/parrish/indexrefraction-seawater-and-freshwater-function-wavelength-andtemperature (last accessed 20 June 2025).

Pfeifer, N., Mandlburger, G., Otepka, J. and Karel, W. (2014). Opals – a framework for airborne laser scanning data analysis. *Computers, Environment and Urban Systems, 45*, pp. 125–136.

Popielarczyk, D. (2016). Accuracy of vertical trajectory determination of hydrographic survey unit using robotized total station. *International Multidisciplinary Scientific GeoConference: SGEM 2*, Albena, Bulgaria, pp. 39–45.

Pöppl, F., Neuner, H., Mandlburger, G. and Pfeifer, N. (2023). Integrated trajectory estimation for 3D kinematic mapping with GNSS, INS and imaging sensors: A framework and review. *ISPRS Journal of Photogrammetry and Remote Sensing, 196*, pp. 287–305. https://doi.org/10.1016/j.isprsjprs.2022.12.022

Pöppl, F., Ullrich, A., Mandlburger, G. and Pfeifer, N. (2024). A flexible trajectory estimation methodology for kinematic laser scanning. *ISPRS Journal of Photogrammetry and Remote Sensing, 215*, pp. 62–79. https://doi.org/10.1016/j.isprsjprs.2024.06.014

Pöppl, F., Ullrich, A., Mandlburger, G. and Pfeifer, N. (2025). Precise and efficient high-frequency trajectory estimation for LiDAR georeferencing. ISPRS Journal of Photogrammetry and *Remote Sensing, 223*, pp. 344–361. https://doi.org/10.1016/j.isprsjprs.2025.03.007

Ressl, C., Kager, H. and Mandlburger, G. (2008). Quality checking of ALS projects using statistics of strip differences. *International Archives of Photogrammetry and Remote Sensing, 37*(B3b), pp. 253–260.

RIEGL (2021). *RIEGL VQ840-G.* RIEGL Laser Measurement Systems GmbH, Austria.

Skaloud, J. and Lichti, D. (2006). Rigorous approach to bore-sight self-calibration in airborne laser scanning. *ISPRS Journal of Photogrammetry and Remote Sensing, 61*(1), pp. 47–59. https://doi.org/10.1016/j.isprsjprs.2006.07.003

Thalmann, T. and Neuner, H. (2021). Temporal calibration and synchronization of robotic total stations for kinematic multisensor-systems. *Journal of Applied Geodesy, 15*(1), pp. 13–30. https://doi.org/10.1515/jag-2019-0070

Thalmann, T. and Neuner, H. (2024). Sensor fusion of robotic total station and inertial navigation system for 6DoF tracking applications. *Applied Geomatics.* https://doi.org/10.1007/s12518-024-00593-4

Tombrink, G., Dreier, A., Klingbeil, L. and Kuhlmann, H. (2024). Spatio-temporal trajectory alignment for trajectory evaluation. *Journal of Applied Geodesy, 19*(2), pp.321-331. https://doi.org/10.1515/jag-2024-0040

Vaidis, M., Dubois, W., Daum, E., LaRocque, D. and Pomerleau, F. (2023). Uncertainty analysis for accurate ground truth trajectories with robotic total stations. *Proceedings of IEEE/RSJ International Conference on Intelligent Robots and Systems (IROS)*, IEEE, Detroit, MI, USA. https://doi.org/10.48550/arXiv.2308.01553

Wang, J., Yu, X. and Guo, S. (2022). Inversion and characteristics of unmodeled errors in GNSS relative positioning. *Measurement, 195*, pp. 111151. https://doi.org/10.1016/j.measurement.2022.111151.

Zogg, H.-M. and Maar, H. (2020). *Leica Nova MS60.* White Paper, Leica Geosystems AG.

https://doi.org/10.58440/ihr-31-2-a14

Authors' biographies

Lucas Dammert is working as a PhD student at TU Wien on the trajectory estimation of multi-sensor systems (primarily unmanned airborne systems) using robotic total stations in a joint position between the groups of photogrammetry and engineering geodesy. During his B.Sc. and M.Sc. he studied Geodesy and Geoinformation in Dresden and Hamburg with a specialization in hydrography. His research interests lie in the fields of hydrography, photogrammetry and engineering geodesy with a focus on kinematic multi-sensor systems.



Lucas Dammert

Florian Pöppl holds an MSc in Technical Mathematics from TU Wien and wrote his PhD dissertation in Geodesy and Geoinformation on trajectory estimation and integration of satellite and inertial navigation with laser scanning. He is currently heading software development at *RIEGL* Laser Measurement Systems GmbH, where he also continues his work on laser scanning data processing, navigation, sensor orientation and calibration.



Florian Pöppl

Jan Rhomberg-Kauert is a PhD student at TU Wien, working as a research assistant in the Department of Geodesy and Geoinformation. With a broad background in mathematics, computational biology and computer science, Jan currently focuses on developing innovative methodologies to improve hydrographic data classification and LiDAR signal processing. His research aims to enhance the understanding of full waveform bathymetric LiDAR with a focus on aquatic vegetation. There he actively engages with various academic and industry partners, contributing to different projects related to hydrography, photogrammetry and airborne LiDAR.



Jan Rhomberg-Kauert

Tomas Thalmann received his DI in Geodesy from TU Wien in 2015. Since then, he worked in several research projects dealing with inertial navigation, laser scanning and robotic total stations at the research group Engineering Geodesy. Focusing on kinematic multi-sensor-systems and time-synchronization, he currently works on enhancing multi-sensor-systems by fusion of inertial sensors and robotic total stations. Since 2020 he is also employed as a surveying engineer and project manager at Vermessung Thalmann.



Tomas Thalmann

https://doi.org/10.58440/ihr-31-2-a14



David Monetti

David Monetti holds a DI from the TU Vienna. He is currently CEO at Skyability GmbH, a drone service provider based in Austria. He manages daily business and research projects funded by the Austrian national funds. His product development activities focus on lidar systems; using lidar on different platforms like ULS, MLS or TLS have turned it into a tool used daily which now creates the best obtainable digital twin of a target of interest. For more than a year now David is also responsible for implementing lidar-bathymetry at Skyability. His research activities and 5+ years hands-on work have turned him into a true expert in the field.



Hans-Berndt Neuner

Univ. Prof. Dr.-Ing. Hans-Berndt Neuner leads the research group engineering geodes at TU Wien. He wrote his dissertation at the geodetic institute of Leibnitz Universität Hannover in the field of deformation analysis and time series analysis and worked there afterwards as a PostDoc. His expertise lies in geometric modelling and analysis of point-based and space-continuous deformation, filter methods in object space and kinematic measurement systems.



Gottfried Mandlburger

Univ. Prof. Dipl.-Ing. Dr. techn. Gottfried Mandlburger studied geodesy at TU Wien, where he also received his PhD in 2006 and habilitated in photogrammetry with a thesis on "Bathymetry from active and passive photogrammetry" in 2021. In April 2024 he was appointed University Professor for Optical Bathymetry at TU Wien. His main research areas are airborne topographic and bathymetric LiDAR from crewed and uncrewed platforms, multimedia photogrammetry, bathymetry from multispectral images, and scientific software development. Gottfried Mandlburger is chair of the DGPF working group LiDAR and Austrians scientific delegate in EuroSDR. He received best paper awards from ISPRS and ASPRS for recent publications on bathymetry from active and passive photogrammetry.

https://doi.org/10.58440/ihr-31-2-a14